Journal of ELECTRONIC MATERIALS
DOI: 10.1007/s11664-017-5803-3
© 2017 The Minerals, Metals & Materials Society

CrossMark

Opto-Electronic Properties of Cu_2ZnSnS_4 Thin Films Grown by Ultrasonic Spray Pyrolysis

K.G. DEEPA,[1,3] T.H. SAJEESH,[2] and NAGARAJU JAMPANA[1]

1.—Department of Instrumentation and Applied Physics, Indian Institute of Science, Bangalore, Karnataka 560012, India. 2.—Department of Physics, St. Alberts's College, Ernakulam 682018, India. 3.—e-mail: deepachaithanya@gmail.com

Cu_2ZnSnS_4 (CZTS) films are deposited by ultrasonic spray pyrolysis technique for photovoltaic applications. The optoelectronic properties are studied by varying Zn and Sn compositions in the film. Films showed a tetragonal kesterite structure with preferential orientation along the (112) plane. The sample with the highest Cu concentration showed the lowest band gap of 1.46 eV. The grain size of the films is greater than 1 μm. Temperature-dependent conductivity studies revealed the presence of defects such as V_{Cu}, V_S, V_{Sn}, Cu_{Zn}, Zn_{Cu}, Zn_{Sn} and Sn_{Zn} in the films. The sample with a Cu/(Zn + Sn) ratio of 0.75 showed Cu-poor and Zn-rich composition and better opto-electronic properties. The sample has *p*-type conductivity with a resistivity of 12 Ω cm. A [V_{Cu}–Zn_{Cu}] defect complex is identified in this sample along with a Zn_{Sn} acceptor level which is favorable for solar cells.

Key words: Thin films, ultrasonic spray pyrolysis, solar cell material, intrinsic defects

INTRODUCTION

I–III–VI_2 semiconductors possess special properties which find application in opto-electronic devices such as solar cells, optical parametric oscillators, light-emitting diodes, laser diodes and non-linear optical devices. Semiconductors such as $CuInSe_2$, $CuInS_2$, $CuGaSe_2$ and $AgInS_2$ are used as absorber layers in solar cells. Among this, $CuInSe_2$-based thin film solar cells possess the highest efficiency of 20%.[1] The cost of indium and the toxicity of Se are the major drawbacks of this material. Cu_2ZnSnS_4 (CZTS) is identified as an alternative for $CuInSe_2$. The constituent elements are non-toxic and abundant in nature. CZTS occurs in kesterite, stannite and primitive mixed Cu-Au-like (PMCA) structures.[2] This kesterite structure has lower energy and high stability. This structure is derived from $CuInSe_2$ by replacing two indium atoms by one Zn and one Sn atom. CZTS exhibits properties similar to $CuInSe_2$ and thus could be considered as an efficient substitute for $CuInSe_2$. The band gap of CZTS (~1.5 eV) matches well with the requirement for a solar cell absorber. In addition, the absorption coefficient (~10^5 cm^{-1}) is high in CZTS, which minimizes the material requirement.

A CZTS thin film solar cell has achieved efficiencies up to 9.1%.[3] Selenization of CZTS thin films helped in increasing the efficiency to 12.6% using a solution-based method.[4] CZTS thin films are deposited using different techniques such as CVD, thermal evaporation, chemical spray pyrolysis, pulsed laser deposition, sputtering, atomic layer deposition and chemical bath deposition.[5–11] Among these techniques , spray pyrolysis is one of the versatile chemical methods used in the deposition of thin films. CZTS thin films are grown using pneumatic spray pyrolysis by different groups, and a maximum efficiency of 5.1% has been achieved with the incorporation of Se.[12–17] A few reports are available on ultrasonic spray pyrolysis also.[18,19] Here, CZTS thin films are grown using an ultrasonic spray pyrolysis technique which is a modified technique of chemical spray pyrolysis. We have indigenously developed an automated spray pyrolysis system and

(Received December 15, 2016; accepted September 13, 2017)

Published online: 24 September 2017

carried out initial studies by varying Sn concentrations.[20,21] Further characterizations are carried out by varying Zn and Sn concentration to get device-quality films.

MATERIALS AND METHODS

The deposition is carried out using an indigenously developed automated ultrasonic spray pyrolysis setup which is described elsewhere.[20] An ultrasonic nebulizer of 1.7-MHz frequency is used for the film deposition. The distance between the spray nozzle and substrate is maintained at 3 cm. 0.06 M $CuCl_2$, 0.04 M $ZnCl_2$, 0.04 M $SnCl_4$ and 0.4 M $SC(NH_2)_2$ are taken as precursor solutions and the substrate temperature is maintained at 440°C. Initial molarities are taken based on the preliminary studies. Zn and Sn concentrations are varied out to obtain device-quality films. Table I shows the molarity of the precursor and the sample name.

X-ray diffraction (XRD) patterns of the samples were recorded using a Bruker D8 instrument operated at 40 kV and 40 mA. A Cu Kα line of wavelength at 1.5405 Å was used as the radiation source and the patterns were recorded in a θ–2θ configuration. Raman spectra were recorded using a Jobin–Yvon LabRAM instrument with an argon ion laser of wavelength 514 nm as the excitation source. Absorption spectra were recorded using an UV–Vis spectrophotometer (SPECORD S600 UV–VIS) over a wavelength of 400–1100 nm. Energy dispersive x-ray analysis (EDX) and scanning electron microscopy (SEM) were carried out under an acceleration voltage of 25 kV. Thickness of the samples were measured using a Bruker Dektak XT surface profilometer. Hall effect measurements were taken using an Ecopia HMS5000. Silver paste was used to make contacts and a magnetic field of strength 0.5 T was applied to the films. Temperature-dependent conductivity measurements were carried out using a Keithley2401 source measure unit and a custom-made conductivity cell (Prompt Eng.).

RESULTS AND DISCUSSIONS

EDX results of the CZTS films are presented in Table I. Sn concentration varied from 17.5% to 9.3% with reduction in the Sn molarity from 0.04 M to 0.02 M. The S percentage was also found to be reduced in proportion with Sn concentration in these samples. The lower concentration of Sn creates a vacancy of Sn (V_{Sn}) acceptor states with a net charge of (2^-) or (4^-). The extra charge may be compensated for with the creation of a sulfur vacancy (V_S^{2+} or $2V_S^{2+}$) to maintain overall valence neutrality. This explains the observed reduction in sulfur in proportion to Sn concentration. For an efficient CZTS solar cell, Cu-poor and Zn-rich conditions are found to be favorable when the [Cu/(Zn + Sn)] ratio is between 0.75 and 1.[22] A Cu-poor condition is preferred in order to avoid the formation of a Cu_{Zn} acceptor level, which lies deep in the band gap and, hence, does not contribute to the carrier separation. A Cu-poor condition aids in the formation of a V_{Cu} acceptor which is a shallow level.[2] An increase in Zn molarity from 0.4 to 0.5 resulted in a Cu-poor and Zn-rich composition with a Cu/(Zn + Sn) ratio of 0.75. Slight increase in Sn molarity resulted in an equal percentage of Zn and Sn in samples CZTS5 and CZTS6.

XRD patterns (Fig. 1) of the films showed a kesterite Cu_2ZnSnS_4 phase (JCPDS 26-0575) with preferential orientation along the (112) plane. Additional peaks corresponding to the (200), (220) and (312) planes of CZTS are observed in the films. Samples CZTS2 and CZTS3 exhibited peaks at 33°, 46.3° and 54.9° which correspond to a Cu_2S phase (JCPDS 12-0227). These samples have higher concentration of Cu, leading to the formation of Cu_2S. The crystallinity is highest for CZTS4. Raman spectroscopy (Fig. 2) was also carried out in order to find out the different phases existing in the films. Samples showed prominent peaks at 335 cm^{-1}

Table I. Sample details

Molarity in the precursor	Sample name
Cu06Zn04Sn04S0.4	CZTS1
Cu06Zn04Sn03S0.4	CZTS2
Cu06Zn04Sn02S0.4	CZTS3
Cu06Zn05Sn03S0.4	CZTS4
Cu06Zn05Sn035S0.4	CZTS5
Cu06Zn05Sn04S0.4	CZTS6

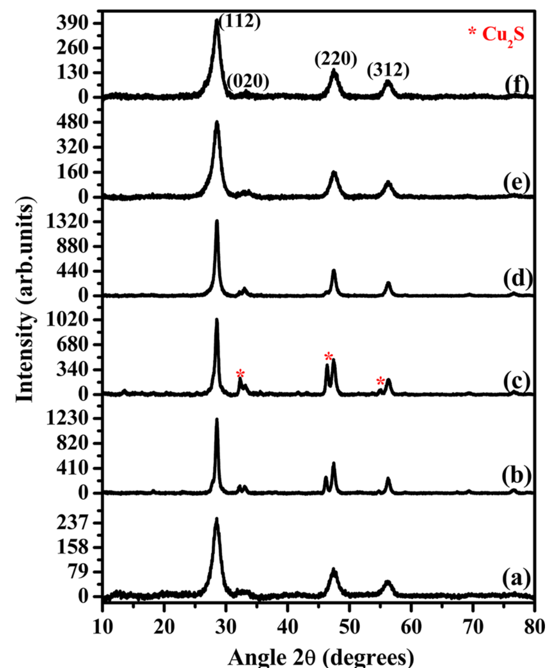

Fig. 1. X-ray diffraction patterns of (a) CZTS1, (b) CZTS2, (c) CZTS3, (d) CZTS4, (e) CZTS5 and (f) CZTS6.

which corresponds to the A1 mode of the tetragonal kesterite CZTS.[23] In CZTS2 and CZTS3, an additional peak appears at 472 cm^{-1} which is attributed to the Cu_2S phase.[24] The Cu_2S phase is reported to appear even in the slightly Cu-rich CZTS films.[17]

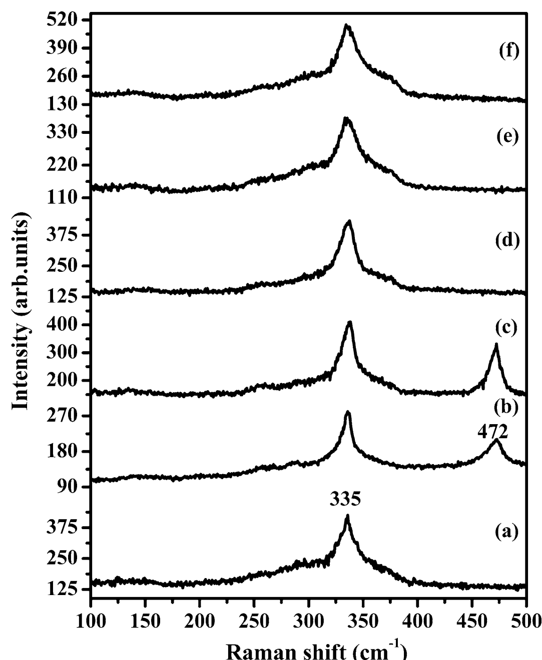

Fig. 2. Raman spectra of (a) CZTS1, (b) CZTS2, (c) CZTS3, (d) CZTS4, (e) CZTS5 and (f) CZTS6.

Raman analysis was found to be in agreement with the crystalline phases determined from XRD.

Band gap of the films are determined using absorption spectra by plotting $(\alpha h\nu)^2$ versus $h\nu$. The intercept of the linear region of the plot in the x-axis gives the value of band gap, as shown in Fig. 3. CZTS is well known as a direct band gap semiconductor. The calculated band gap values are given in Table II. Band gap varies from 1.42 eV to 1.56 eV with variation in composition, in agreement with the literature.[18] In CZTS, the uppermost valence band is formed by Cu-d and S-p states, similar to $CuInSe_2$. The lower conduction band is formed by hybridization of the sulfur s, p and Sn s states.[25] The reduction in the energy band gap of the Cu-rich sample CZTS3 may be the result of p–d hybridization between S 4p and Cu 3d states. The lesser energy separation between these states repels the valence band maximum upwards, allowing reduction in the band gap.[26] CZTS3 has comparatively low absorption.

SEM images of CZTS films (Fig. 4) show square-shaped grains. In CZTS3, flake-shaped structures are also seen, which may be due to the presence of Cu_2S phase. Cu-rich films CZTS1 to CZTS3 have grain size $\sim$ 1.4 μm and it varies slightly among CZTS4 to CZTS6. The crystallite size is also calculated using the Debye–Scherrer formula:

$$L = \frac{0.9\lambda}{\beta \cos\theta}$$

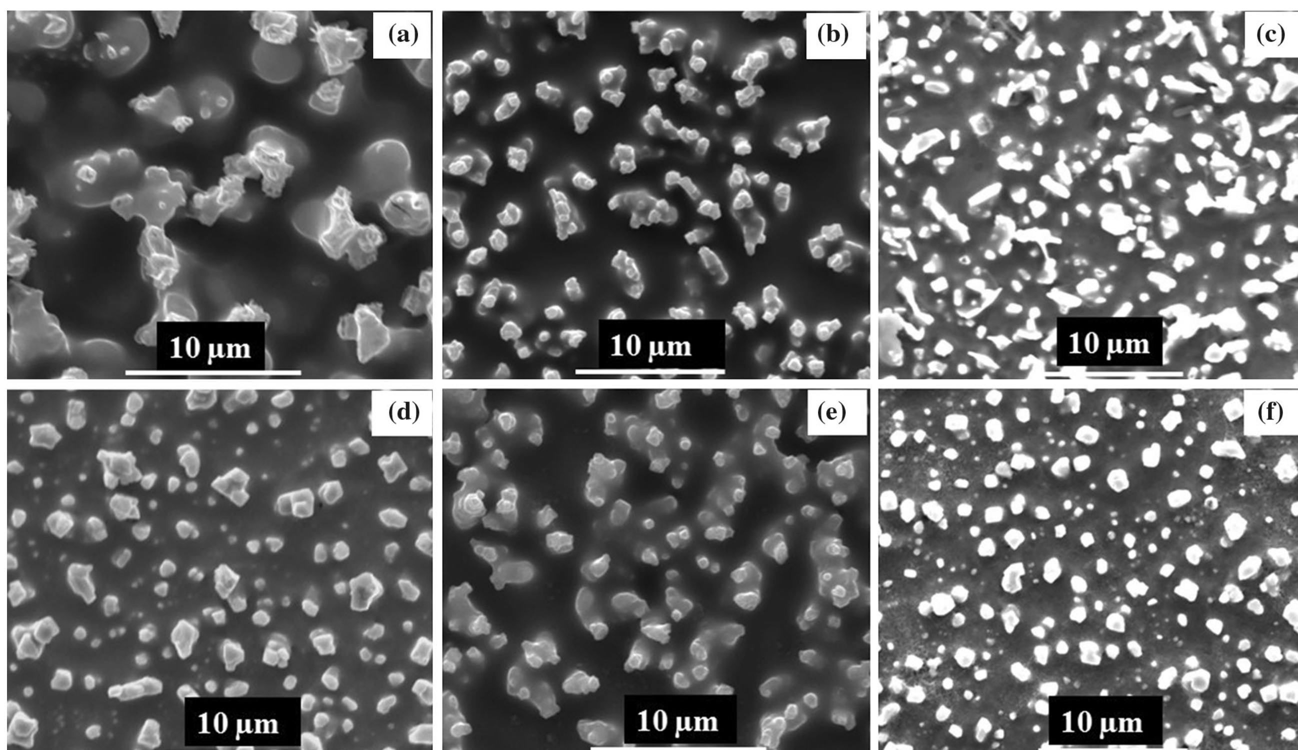

Fig. 3. SEM images of (a) CZTS1, (b) CZTS2, (c) CZTS3, (d) CZTS4, (e) CZTS5 and (f) CZTS6.

Table II. Properties of Cu_2ZnSnS_4 thin films

Sample details	Cu/(Zn + Sn)	Atomic percentage				Band gap (eV)	Gain size (μm)	FWHM (°)	Crystallite size (nm)
		Cu	Zn	Sn	S				
CZTS1	0.94	25.1	9.3	17.5	48.1	1.43	1.46	1.414	6
CZTS2	0.87	26.1	17.8	12.2	43.9	1.42	1.4	0.516	14
CZTS3	1.13	31.5	18.5	9.3	40.7	1.43	1.4	0.49	17
CZTS4	0.75	23.4	18.4	12.7	45.5	1.52	1.2	0.624	13
CZTS5	0.65	20.3	15.4	15.7	48.6	1.51	1.17	1.382	6
CZTS6	0.50	18.0	17.1	18.6	46.3	1.56	1.1	1.419	6

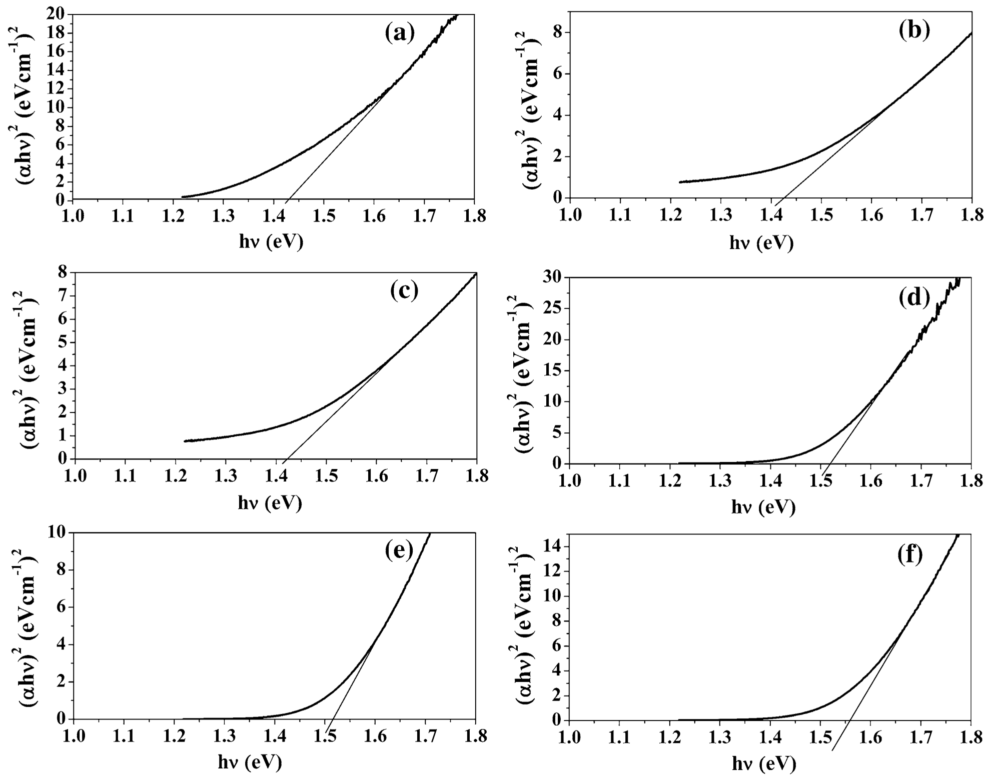

Fig. 4. Absorption spectra of (a) CZTS1, (b) CZTS2, (c) CZTS3, (d) CZTS4, (e) CZTS5 and (f) CZTS6.

where λ is the wavelength of the x-ray (1.5405 Å in the present case), β is the full width at half maximum (FWHM) of the peak and θ is the diffraction angle. The FWHM and corresponding crystallite size are given in Table II. The size varies from 6 nm to 17 nm, which is entirely different from the grain size obtained using SEM. It is assumed that the grains are composed of many crystallites and, hence, have a bigger size.

Electrical characterization of the samples are performed using a Hall effect measurement system and the values are given in Table III. Except for CZTS6, all others showed *p*-type conductivity. The lower formation energy of acceptor defects makes *p*-type doping of CZTS easier.[27] The resistivity varied from 0.2 Ω cm to 10^7 Ω cm. The resistivity is found to be highly dependent on Cu concentration. CZTS3 has the highest percentage of Cu and lowest resistivity. With reduction of the Cu concentration, resistivity increased gradually and the conductivity type changed to *n*-type for CZTS6. Carrier concentrations in the samples CZTS1 to CZTS4 are in the order of 10^{16}/cm^3. The resistive samples CZTS5 and CZTS6 showed slightly lower values, of the order 10^{15}/cm^3. Carrier mobility varied from 4.2 cm^2/Vs to 13.6 cm^2/Vs in the *p*-type samples CZTS1 to CZTS5, and for CZTS6, it is 0.57 cm^2/Vs. The higher mobility in CZTZ2 and CZTS3 could be attributed

Table III. Electrical properties of CZTS films

Sample details	Resistivity (Ω cm)	Type of conductivity	Carrier concentration (ions/cm^3)	Mobility (cm^2/Vs)
CZTS1	26	*p*	1.3×10^{16}	9.5
CZTS2	7	*p*	5.2×10^{16}	12.3
CZTS3	0.2	*p*	8.4×10^{16}	13.6
CZTS4	12	*p*	4.7×10^{16}	10.8
CZTS5	5×10^4	*p*	8×10^{15}	4.2
CZTS6	2×10^7	*n*	3.2×10^{15}	0.57

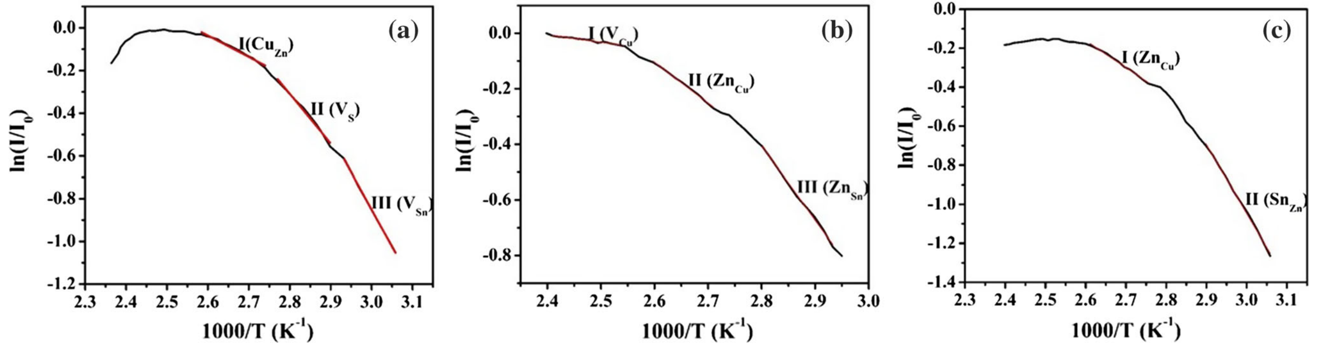

Fig. 5. Arrhenius plots of (a) CZTS3, (b) CZTS4 and (c) CZTS6.

to the presence of Cu_2S phase which is highly conductive.

In order to study the defect levels present in CZTS thin films, temperature-dependent resistivity measurements were carried out from 305 K to 450 K on samples CZTS3 (Cu-rich), CZTS4 (optimized) and CZTS6 (*n*-type Cu-poor). The relation between the conductivity of the sample and the temperature is

$$\sigma = \sigma_0 \exp\left({-E_{\rm a}}/{kT} \right) \quad (1)$$

where E_a is the activation energy (or enthalpy) of the process and k is the Boltzmann constant.

The activation energy is calculated from the slope of ln (σ) versus 1000/T (Arrhenius plot). The changes in slope at different regions of temperature indicate a variation in the activation process, i.e., activation energy due to thermal excitation of impurities situated at different levels in the band gap.

Figure 5 shows the Arrhenius plot for the selected CZTS samples and Table IV gives different defect levels identified. The regions are marked as I, II and III according to the change in slope of the graph. CZTS3 showed activation energies of 87 meV, 200 meV and 300 meV which are assigned to Cu_{Zn}, V_S and V_{Sn}, respectively.[28] Cu_{Zn} and V_{Sn} are acceptor states which contributes to the *p*-type conductivity and V_S is a donor. From Table II, it is clear that CZTS3 is Cu-rich, which facilitates the formation of a Cu_{Zn} defect level which has lower formation energy. Lower concentrations of Sn and S have resulted in the formation of V_S and V_{Sn} levels.

Table IV. Activation energies and corresponding defects in CZTS

Sample name	Activation energy (meV)
CZTS3	87-Cu_{Zn}
	200-V_S
	300-V_{Sn}
CZTS4	24-V_{Cu}
	127-Zn_{Cu}
	231-Zn_{Sn}
CZTS6	119-Zn_{Cu}
	296-Sn_{Zn}

In CZTS4, Cu_{Zn} disappeared and the shallow acceptor level, V_{Cu}, is formed with an activation energy of 24 meV. As revealed from EDX analysis, Cu concentration is low in this sample, which supports the formation of V_{Cu}. The defect level with an activation energy of 127 meV is assigned to the donor defect Zn_{Cu}. [V_{Cu}–Zn_{Cu}] defect complex is known as a non-stoichiometric-conserving defect complex.[29] The formation energy of this defect complex is less than the formation energy of the individual defects under Cu-poor and Zn-rich conditions. The shallow defect pair [V_{Cu}–Zn_{Cu}] is found to be favorable for solar cells since it lowers the conduction and valence band edges.[22] In CZTS4, an activation energy of 231 meV, corresponding to the acceptor defect Zn_{Sn}, was also calculated. In CZTS6, which exhibited *n*-type conductivity, donor-type defects are identified at 119 meV and 296 meV due to Zn_{Cu} and Sn_{Zn}. The

conductivity studies confirms the suitability of CZTS4 for solar cell fabrication.

CONCLUSIONS

CZTS thin films are characterized by varying the Zn and Sn concentrations for the use as an absorber in solar cells. Films deposited in Cu-poor and Zn-rich conditions showed a band gap of 1.55 eV and resistivity of 12 Ω cm. Presence of a $[V_{Cu}–Zn_{Cu}]$ defect pair is identified in this film which favors the charge transportation in solar cells.

ACKNOWLEDGEMENTS

Deepa K.G. thanks the Science and Engineering Research Board (SERB), Department of Science and Technology, Government of India for the assistance through a Young Scientist Start-up grant (YSS/2014/000805). Sajeesh T.H. acknowledges UGC, Govt. of India for the financial support through minor project scheme (1809-MRP/14-15/KLMG007/UGC-SWRO).

REFERENCES

1. D. Herrmann, P. Kratzert, S. Weeke, M. Zimmer, J. Djordjevic-Reiss, R. Hunger, P. Lindberg, E. Wallin, O. Lundberg, and L. Stolt, in *Proceedings of 40th IEEE Photovoltaic Specialists Conference,* vol. 2775 (2014).
2. S. Chen, X.G. Gong, A. Walsh, and S.-H. Wei, *Appl. Phys. Lett.* 94, 041903 (2009).
3. K. Sun, C. Yan, F. Liu, J. Huang, F. Zhou, J.A. Stride, M. Green, and X. Hao, *Adv. Energy Mater.* 6, 1600046 (2016).
4. W. Wang, M.T. Winkler, O. Gunawan, T. Gokmen, T.K. Todorov, Y. Zhu, and D.B. Mitzi, *Adv. Energy Mater.* 4, 1301465 (2013).
5. T. Washio, T. Shinji, S. Tajima, T. Fukano, T. Motohiro, K. Jimbo, and H. Katagiri, *J. Mater. Chem.* 22, 4021 (2012).
6. K. Wang, O. Gunawan, T. Todorov, B. Shin, S.J. Chey, N.A. Bojarczuk, D. Mitzi, and S. Guha, *Appl. Phys. Lett.* 97, 143508 (2010).
7. M. Aono, K. Yoshitake, and H. Miyazaki, *Phys. Status Solidi* 10, 1058 (2013).
8. K. Moriya, K. Tanaka, and H. Uchiki, *Jp. J. Appl. Phys.* 46, 5780 (2007).
9. T.P. Dhakal, C.-Y. Peng, R.R. Tobias, R. Dasharathy, and C.R. Westgate, *Solar Energy* 100, 23 (2014).
10. T.R. Rana, N.M. Shinde, and J. Kim, *Mater. Lett.* 162, 40 (2016).
11. E. Thimsen, S.C. Riha, S.V. Baryshev, A.B.F. Martinson, J.W. Elam, and M.J. Pellin, *Chem. Mater.* 24, 3188 (2012).
12. M.E. Rodríguez, J. López-García, D. Sylla, X. Fontané, Y. Sánchez, S. López-Marino, V. Izquierdo-Roca, W. Riedel, W. Ohm, S. Gledhill, O. Vigil-Galán, and E. Saucedo, *Phys. Status Solidi A* 212, 126 (2015).
13. N.M. Shinde, R.J. Deokate, and C.D. Lokhande, *J. Anal. Appl. Pyrol.* 100, 12 (2013).
14. Y.B.K. Kumar, P.U. Bhaskar, G.S. Babu, and V.S. Raja, *Phys. Status Solidi A* 207, 149 (2010).
15. X. Zeng, K.F. Tai, T.L. Zhang, C.W.J. Ho, X. Chen, A. Huan, T.C. Sum, and L.H. Wong, *Sol. Energy Mater. Sol. Cells* 124, 55 (2014).
16. N. Nakayama and K. Ito, *Appl. Surf. Sci.* 92, 171 (1996).
17. V.G. Rajeshmon, M.R.R. Menon, C. SudhaKartha, and K.P. Vijayakumar, *J. Anal. Appl. Pyrol.* 110, 448 (2014).
18. W. Daranfed, M.S. Aida, N. Attaf, J. Bougdira, and H. Rinnert, *J. Alloys Compd.* 542, 22 (2012).
19. S. Guitouni, M. Khammar, M. Messaoudi, N. Attaf, and M.S. Aida, *J. Semicond.* 37, 122001 (2016).
20. K.G. Deepa and J. Nagaraju, *J. Anal. Appl. Pyrol.* 117, 141 (2016).
21. K.G. Deepa, G. Chandrabose, and J. Nagaraju, *J. Anal. Appl. Pyrol.* 120, 356 (2016).
22. S. Chen, A. Walsh, X. Gong, and S. Wei, *Adv. Mater.* 25, 1522 (2013).
23. J.M. Skelton, A.J. Jackson, M. Dimitrievska, S.K. Wallace, and A. Walsh, *APL Mater.* 3, 041102 (2015).
24. B.M. Sukarova, M. Najdoski, I. Grozdanov, and C.J. Chunnilall, *J. Mol. Struct.* 410–411, 267 (1997).
25. M. Jiang and X. Yan. doi:10.5772/50702.
26. J.E. Jaffe and A. Zunger, *Phys. Rev. B.* 29, 1882 (1984).
27. S. Chen, X.G. Gong, A. Walsh, and S.-H. Wei, *Appl. Phys. Lett.* 96, 021902 (2010).
28. S. Chen, J. Yang, X.G. Gong, A. Walsh, and S.-H. Wei, *Phys. Rev. B* 81, 245204 (2010).
29. M. Kumar, A. Dubey, N. Adhikari, S. Venkatesan, and Q. Qiao, *Energy Environ. Sci.* 8, 3134 (2015).